ORIGINAL ARTICLE

Influence of CO_2 migration from geological storage on the chemical composition of groundwater and monitoring indicators

Lian Li[1] · Yahong Wu[1] · Shan Chong[2] · Qingzhi Wen[3] · Qianguo Lin[4] · Shuo Zhang[5]

Abstract

In the process of CO_2 geological sequestration, there is a risk that CO_2 will leak into groundwater, resulting in a series of physical and chemical reactions, with influence on chemical compositions of groundwater. In this work, numerical simulation is conducted to study the influence of CO_2 migration on the chemical composition of groundwater. The modeling results indicated that when CO_2 leaks into groundwater, gaseous CO_2 will migrate upward and diffuse laterally under the effect of buoyancy. The acidity of groundwater is enhanced and the pH is significantly reduced, leading to dissolution of calcite, illite, oligoclase, K-feldspar, chlorite and hematite, and precipitation of quartz, kaolinite, smectite-Na, siderite and smectite-Ca. The porosity of the formation increases. The concentrations of K^+ and Fe^{2+} in groundwater gradually increase, the concentrations of Ca^{2+} and HCO_3^- basically remain unchanged after increasing to a certain value, the concentrations of Mg^{2+} and AlO_2^- first increase and then decrease, and the concentrations of Na^+, Cl^- and SO_4^{2-} first decrease slightly and then gradually increase, but the change in concentration is small. Therefore, Fe^{2+}, Mg^{2+}, Ca^{2+} and pH can be used as important monitoring indicators of whether CO_2 leakage into groundwater during geological storage.

Keywords Geological storage · CO_2 migration · Groundwater · Chemical composition · Monitoring indicators · TOUGHREACT

Introduction

With the increasing concerns on global warming, CO_2 geologic sequestration has been considered to be one of the most effective ways to reduce CO_2 emissions and alleviate global warming (Cao et al. 2021). However, due to the uncertainty in geological conditions, the risk of CO_2 leaking during geological storage has to be considered (Aines et al. 2009; Oldenburg et al. 2011). For example, sequestered CO_2 may migrate into groundwater along faults, fractures and recovery wells (Du et al. 2012; Xie et al. 2017). Once CO_2 migrate into groundwater, it will break the original hydrochemical equilibrium in groundwater and cause a series of problems on groundwater quality (Apps et al. 2010). Therefore, studying the impact of CO_2 migration from geological storage on the quality of groundwater is an important part of the environmental risk assessment and development of early warning in CO_2 geological storage.

Although the evaluation of the impact of CO_2 geological storage on water quality has been studied long ago (Meer 1992), systematic study of the impact of CO_2 on shallow groundwater quality began in 2004. Wang and Jaffe (2004) used numerical simulation for the first time to study the impact of CO_2 migration on shallow groundwater. The results showed that if the monitored trace metal indicators

✉ Shan Chong
396185870@qq.com

1 State Key Laboratory of Petroleum Resources and Prospecting, China University of Petroleum (Beijing), Beijing 102249, China

2 State Key Laboratory of Coal Resources and Safe Mining, China University of Mining and Technology (Beijing), Beijing 100083, China

3 Innovation Center for Engineering Science and Advanced Technology, College of Engineering, Peking University, Beijing 100871, China

4 Laboratory of Carbon Dioxide Capture, Suzhou Research Institute of North China Electric Power University, Suzhou 215000, Jiangsu, China

5 State Key Laboratory of Hydroscience and Engineering, Department of Hydraulic Engineering, Tsinghua University, Beijing 100084, China

were abnormal, it could be an indicator of CO_2 leakage to shallow aquifers. Carroll et al. (2009) conducted reactive migration modeling on the impact of CO_2 intrusion into American plateau aquifers, and showed that CO_2 migration in aquifers can be detected by pH and carbonate chemical changes, and pointed out that the most appropriate monitoring location was the bottom of the waterproof roof. Fahrner et al. (2011) used PhreeqC to simulate the impact of CO_2 migration to shallow groundwater on the electrical conductivity (EC) of groundwater, analyzed the impact of CO_2 intrusion on the EC change of groundwater, and explored the use of monitoring groundwater EC changes to identify leakage. Kharaka et al. (2010) monitored the concentration changes of the main components, minor components, trace components and organic components in groundwater after CO_2 injection, and the results showed that with CO_2 injection, the concentrations of chemical components in groundwater changed significantly. Among them, pH dropped from 7.0 to 5.6, alkalinity increased from 400 to 1330 mg/L. The main components and trace components (including Pb, As, etc.) in groundwater increased significantly, but were lower than the Environmental Protection Agency (EPA) drinking water limit in the US. Keating et al. (2010, 2013) studied the impact of CO_2 geological storage on the hydrochemistry of shallow groundwater in sandstone aquifers in New Mexico, USA. The study showed that high alkalinity and carbonate minerals mitigate the effects of CO_2 intrusion on pH, and no migration of trace elements in the aquifer was observed, but the migration of As, U and Pb was observed in other saline aquifers. Therefore, they suggested that geochemical conditions determine the changes in the water quality of the aquifer and also affect the effectiveness of detecting CO_2 migration. Chen (2013) studied the Ordos region of China and used the TOUGHREACT numerical simulation software to simulate the leakage of CO_2 into shallow aquifers, and studied its impact on water quality. The results showed the migration of CO_2 causes the migration of certain metals in the ore, which in turn affected the total amount of metal ions in the water.

Lu et al. (2010) conducted CO_2 injection experiments on actual water-bearing media in the Gulf Coast area of the United States. The results showed the pH in the water decreased sharply (by about 3 units) at the beginning of CO_2 injection, and then gradually recovered to a stable value. The concentration of some metal elements such as Ca, Mg, Zn, etc., increased rapidly when CO_2 was just injected, and then tended to stabilize. The concentration of other metal elements such as Fe, Al, Cu, etc., increased at the beginning of the injection, and then began to decrease and became lower than before the test. Little and Jackson (2010, 2011)

conducted more than 300 days of indoor injection experiments using aqueous media in 17 regions of the United States. The results showed that the H^+ concentration in all aqueous media samples increased by 1 to 2 orders of magnitude. The concentration of alkali elements, alkaline earth elements, Mn, Co, Ni, and Fe in the water increased by more than 2 orders of magnitude. The concentration of U and Ba in individual media samples increased significantly. The migration of trace metal elements, the buffering effect of carbonate minerals, and the redox conditions of shallow aquifers control the effect of CO_2. Because the concentrations of Mn, Fe, and Ca tend to increase at the beginning of the experiment, their concentrations can be used as the basis for monitoring CO_2 leakage. Zhang et al. (2016) studied the impacts on pH value, DO, HCO_3^- and COD of surface water by changing the leakage time, leakage rate, and the temperature of carbon dioxide. They suggested that pH, DO and HCO_3^- could be used as the surface water monitering indicators for CO_2 geological storage.

Natural isotope tracers are an important way to detect CO_2 leakage. Sr isotopes were used to record the dissolution of carbonate rocks at CO_2-enhanced oil recovery sites (Quattrocchi et al. 2005), and were coupled with carbon isotopes to track the movement of CO_2 plumes during a controlled leak of CO_2 into a shallow aquifer (Newell et al. 2014). Kim et al. (2020) evaluated the application of ^{222}Rn in groundwater as a tracer for monitoring CO_2 plume migration on shallow groundwater, and the results indicated that ^{222}Rn could be used as a sensitive tracer to directly monitor CO_2 leakage. Gardiner et al. (2021) demonstrated that multiple isotope system ($\delta^{13}C_{DIC}$, $^{87}Sr/^{86}Sr$, $^{234}U/^{238}U$) could be used to identify and measure the impact of CO_2 leakage at sequestration sites.

CO_2 storage involves the flow of multi-phase and multi-component fluids in geological media, and processes such as mechanical and chemical reactions. To accurately simulate the effects of CO_2 migration on the chemical composition of groundwater, it is necessary to couple the hydrodynamic and chemical reaction processes that may occur during the movement of multi-phase fluids in the formation. In this work, the Yanchang Oilfield in China was studied with numerical simulation to establish the reaction transport model of CO_2 migration to groundwater during geological storage. By analyzing the influence of CO_2 migration during geologic sequestration on the chemical components of groundwater, we can screen out monitoring indicators that are more sensitive to changes of CO_2 leakage, and provide basis for similar CO_2 geological storage monitoring programs, and reduce the possible risks in carbon capture and storage (CCS) projects.

Model setup

Modeling code and conceptualization

The non-isothermal reactive geochemical transport code TOUGHREACT V3.32-OMP (Xu 2001; Xu et al. 2006, 2014) was used in this work. TOUGHREACT is an extension of TOUGH2 (Pruess et al. 1999) and the fluid property module ECO2N was used for H_2O–CO_2–NaCl mixtures (Pruess et al. 2004).

The depth of groundwater in the Yanchang Oilfield in China is 10 m, and the aquifer is sandstone. It is assumed that CO_2 is leaking into the groundwater through cracks in the formation (Fig. 1). The vertical thickness of the groundwater is 60 m, which is divided into 6 grids, and the length in the horizontal direction is 500 m, which is divided into 50 grids (Fig. 2). The volume of the lateral boundary mesh is set to infinity. The annual average ground temperature in this area is 10.8 °C, the temperature gradient is about 3.1 °C /100 m, and the hydrostatic pressure gradient is 10 bar/100 m. Therefore, the bottom temperature of the model is about 13 °C and the pressure is 8 bar. The CO_2 leakage point is set at $X = 250$ m, the CO_2 leaking time and simulation time are set to 100 years. The constant leakage rate of CO_2 is 0.0001 kg/s, which is estimated by the following formula.
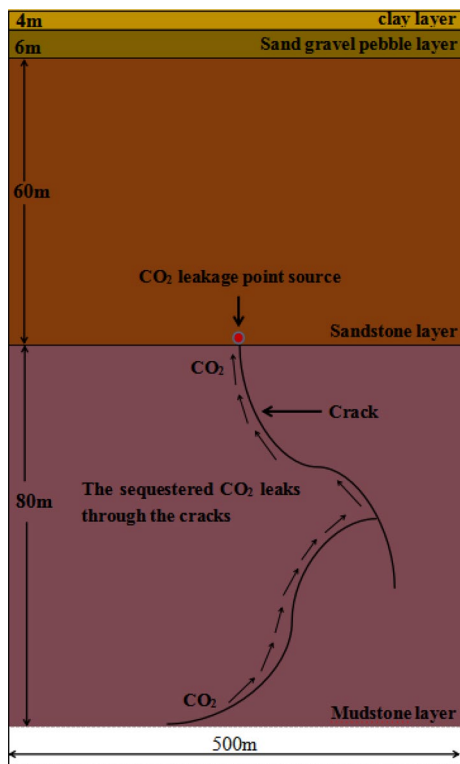

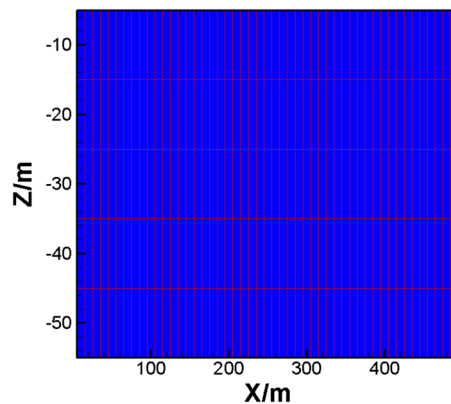**Fig. 1** Diagram of CO_2 leakage

Fig. 2 Scheme of the grid

$$Q_G = C_d APY \sqrt{\frac{MK}{RT} \left(\frac{2}{K+1}\right)^{\frac{K+1}{K-1}}}, \tag{1}$$

where Q_G is the gas leakage rate, kg/s; C_d is the gas leakage coefficient, and $C_d = 1$ when the shape of the crack is round, $C_d = 0.95$ when the shape of the crack is triangular, $C_d = 0.9$ when the shape of the crack is rectangular; A is the area of the crack, m^2; P is the pressure, MPa; Y is the outflow coefficient; M is the relative molecular mass, and the relative molecular mass of CO_2 is 0.044 kg/mol; K is the adiabatic index; R is the gas constant, the value is 8.314, J/(mol·K); T is the temperature, K.

For the hydrogeologic parameters of groundwater, the porosity and permeability values are from geological surveys of the Yanchang oilfield in China, and the other hydrogeological parameters are from Xu et al. (2010). The hydrogeologic parameters are shown in Table 1.

The liquid relative permeability and capillary pressure models applied in this model are the Van Genuchten model (Van Genuchten 1980), and the gas relative permeability model is the Corey model (Corey 1954). The specific parameters are extracted from Xu et al. (2010). The models

Table 1 Hydrogeological parameters

Physical property parameter	Value
Porosity	0.2
Permeabilitym (m^2)	
k_h	0.5×10^{-13}
k_v	0.5×10^{-14}
Thermal conductivity (W/(m °C))	2.51
Rock grain density (kg/m^3)	2600
Coefficient of compressibility (1/pa)	4.5×10^{-10}
Aqueous diffusion coefficient (m^2/s)	1.0×10^{-9}
Rock specific heat (J/(kg °C))	920

Table 2 Models of relative permeability and capillary pressure

Relative permeability

Liquid phase relative permeability (Van Genuchten 1980)

$k_{lr} = \sqrt{S^*}\{1 - (1 - [S^*]^{1/m})^m\}^2$

with $S^* = (S_l - S_{lr})/(1 - S_{lr})$

S_{lr}: Residual water saturation, $S_{lr} = 0.30$
m: Index, $m = 0.457$

Capillary pressure function (Van Genuchten 1980)

$P_{cap} = -P_0([S^*]^{-1/m} - 1)^{1-m}$

$S^* = (S_l - S_{lr})/(1 - S_{lr})$

$P_0 = \rho_w/\alpha$

S_{lr}: Residual water saturation, $S_{lr} = 0.00$
m: Index, $m = 0.457$
P_0: Coefficient of strength, $P_0 = 19.61$ kPa

Gas phase relative permeability (Corey 1954)

$k_{rg} = (1 - \hat{S})^2(1 - \hat{S}^2)$

with $\hat{S} = (S_l - S_{lr})/(S_l - S_{lr} - S_{gr})$

S_{gr}: Residual gas saturation, $S_{gr} = 0.50$

Table 3 List of mineral composition

Mineral	Chemical composition	Volume fraction (%)
Primary mineral		
Calcite	$CaCO_3$	1.929
Quartz	SiO_2	57.888
Kaolinite	$Al_2Si_2O_5(OH)_4$	2.015
Illite	$K_{0.6}Mg_{0.25}Al_{1.8}(Al_{0.5}Si_{3.5}O_{10})(OH)_2$	0.954
Oligoclase	$CaNa_4Al_6Si_{14}O_{40}$	19.795
K-feldspar	$KAlSi_3O_8$	8.179
Chlorite	$Fe_{2.5}Mg_{2.5}Al_2Si_3O_{10}(OH)_8$	4.556
Smectite-Na	$Na_{0.290}Mg_{0.26}Al_{1.77}Si_{3.97}O_{10}(OH)_2$	3.897
Hematite	Fe_2O_3	0.497
Secondary mineral		
Magnesite	$MgCO_3$	0
Siderite	$FeCO_3$	0
Pyrite	FeS_2	0
Albite	$NaAlSi_3O_8$	0
Smectite-Ca	$Ca_{0.145}Mg_{0.26}Al_{1.77}Si_{3.97}O_{10}(OH)_2$	0
Dolomite	$CaMg(CO_3)_2$	0
Ankerite	$CaMg_{0.3}Fe_{0.7}(CO_3)_2$	0
Dawsonite	$NaAlCO_3(OH)_2$	0

of relative permeability and capillary pressure are shown in Table 2.

The mineral composition of the formation

The primary mineral composition of the aquifer and the possible secondary minerals are shown in Table 3, extracted from Xu et al. (2014).

The volume fractions of primary mineral, possible secondary mineral, and their reaction kinetics parameters are shown in Table 4. Since the reaction rate of calcite is fast, it is assumed at equilibrium throughout the simulations. The dissolution and precipitation of other minerals are controlled by kinetics, and the kinetic parameters are extracted from Lasaga et al. (1994).

Kinetic rates could be functions of non-basis species as well. Usually the species appearing in rate laws happen to be basis species. TOUGHREACT (Xu et al. 2006) uses a general form of rate expression (Lasaga et al. 1994).

$$r_n = f(c_1, c_2, \ldots, c_{N_c}) = \pm k_n A_n \left| 1 - \Omega_n^\theta \right|^\eta \quad n = 1, 2 \ldots N_q, \tag{2}$$

where positive values of r_n indicate dissolution, and negative values precipitation, k_n is the rate constant, A_n is the specific reactive surface area per kg H_2O, Ω_n is the kinetic mineral saturation ratio. θ and η are usually taken equal to one.

The temperature dependence of the reaction rate constant can be expressed reasonably well via an Arrhenius equation (Lasaga, 1984; Steefel and Lasaga, 1994). Because many rate constants are reported at 25 °C, it is convenient to approximate rate constant dependency as a function of temperature, thus

$$k = k_{25}\exp\left[\frac{-E_a}{R}\left(\frac{1}{T} - \frac{1}{298.15}\right)\right], \tag{3}$$

where k_{25} is the rate constant at 25 °C; R is gas constant; E_a is the activation energy; T is absolute temperature.

The reaction rate constant calculated using the above formula is usually considered only with pure water (neutral mechanism), while the dissolution and precipitation of minerals are often catalyzed by H^+ (acid mechanism) and OH^- (base mechanism). The kinetic rate constant k includes each of these three mechanisms (Lasaga et al. 1994; Palandri and Kharaka 2004).

Table 4 Mineral composition and reaction kinetics parameters in the model

Mineral	A (cm²/g)	Parameters for kinetic rate law							
		Neutral mechanism		Acid mechanism			Base mechanism		
		K_{25} (mol/m²/s)	E_a (KJ/mol)	K_{25} (mol/m²/s)	E_a (KJ/mol)	n (H⁺)	K_{25} (mol/m²/s)	E_a (KJ/mol)	n (H⁺)
Primary mineral									
Calcite	Assumed at equilibrium								
Quartz	9.8	1.023×10^{-14}	87.7						
Kaolinite	151.6	6.918×10^{-14}	22.2	4.898×10^{-12}	65.9	0.777	8.813×10^{-18}	17.9	-0.472
Illite	151.6	1.660×10^{-13}	35	1.047×10^{-11}	23.6	0.34	3.020×10^{-17}	58.8	-0.4
Oligoclase	9.8	1.445×10^{-13}	69.8	2.138×10^{-11}	65.0	0.457			
K-feldspar	9.8	3.890×10^{-13}	38	8.710×10^{-11}	51.7	0.5	6.310×10^{-22}	94.1	-0.823
Chlorite	9.8	3.020×10^{-13}	88	7.762×10^{-12}	88	0.5			
Smectite-Na	151.6	1.660×10^{-13}	36	1.047×10^{-11}	23.6	0.34	3.020×10^{-17}	58.8	-0.4
Hematite	12.9	2.512×10^{-15}	66.2	4.074×10^{-10}	66.2	1			
Secondary mineral									
Magnesite	9.8	4.571×10^{-10}	23.5	4.169×10^{-7}	14.4	1			
Siderite	9.8	1.260×10^{-9}	62.76	6.457×10^{-4}	36.1	0.5			
Pyrite	12.87			2.818×10^{-5}	56.9	0.5	3.020×10^{-8}	56.9	-0.5
Albite	9.8	2.754×10^{-10}	69.8	6.918×10^{-11}	65.0	0.457	2.512×10^{-16}	71	-0.572
Smectite-Ca	151.6	1.660×10^{-13}	35.0	1.047×10^{-11}	23.6	0.34	3.020×10^{-17}	58.8	-0.4
Dolomite	9.8	2.951×10^{-8}	52.2	6.457×10^{-4}	36.1	0.5			
Ankerite	9.8	1.260×10^{-9}	62.76	6.457×10^{-4}	36.1	0.5			
Dawsonite	9.8	1.260×10^{-9}	62.76	6.457×10^{-4}	36.1	0.5			

$$k = k_{25}^{nu} \exp\left[\frac{-E_a^{nu}}{R}\left(\frac{1}{T} - \frac{1}{298.15}\right)\right]$$
$$+ k_{25}^{H} \exp\left[\frac{-E_a^{H}}{R}\left(\frac{1}{T} - \frac{1}{298.15}\right)\right] a_H^{n_H} \qquad (4)$$
$$+ k_{25}^{OH} \exp\left[\frac{-E_a^{OH}}{R}\left(\frac{1}{T} - \frac{1}{298.15}\right)\right] a_{OH}^{n_{OH}},$$

where superscripts or subscripts nu, H, and OH indicate neutral, acid and base mechanisms, respectively; E_a is the activation energy, (KJ/mol); k_{25} is the rate constant at 25 °C, (mol/(m² s)); R is gas constant, (KJ/(mol K)); T is absolute temperature, (K); a is the activity of the species; and n is power term (constant). Notice that parameters θ and η are assumed the same for each mechanism.

The reaction surface area A changes as the reaction progresses. In TOUGHREACT, the reaction surface area is approximated as a spherical model.

$$A = \frac{(1-\phi)}{\phi}\frac{3}{r}, \qquad (5)$$

where ϕ is porosity, r is the particle radius of a particular porous medium.

Chemical composition of shallow groundwater

The initial chemical composition is measured using groundwater samples collected from the Yanchang Oilfield in China. The salinity of groundwater is about 0.867 g/L and the density is 1×10^3 kg/m³. The groundwater is reacted with aquifer minerals listed in Table 3 to obtain equilibrium concentration. The initial and equilibrium concentrations are given in Table 5.

Table 5 Initial concentration of chemical compositions in groundwater

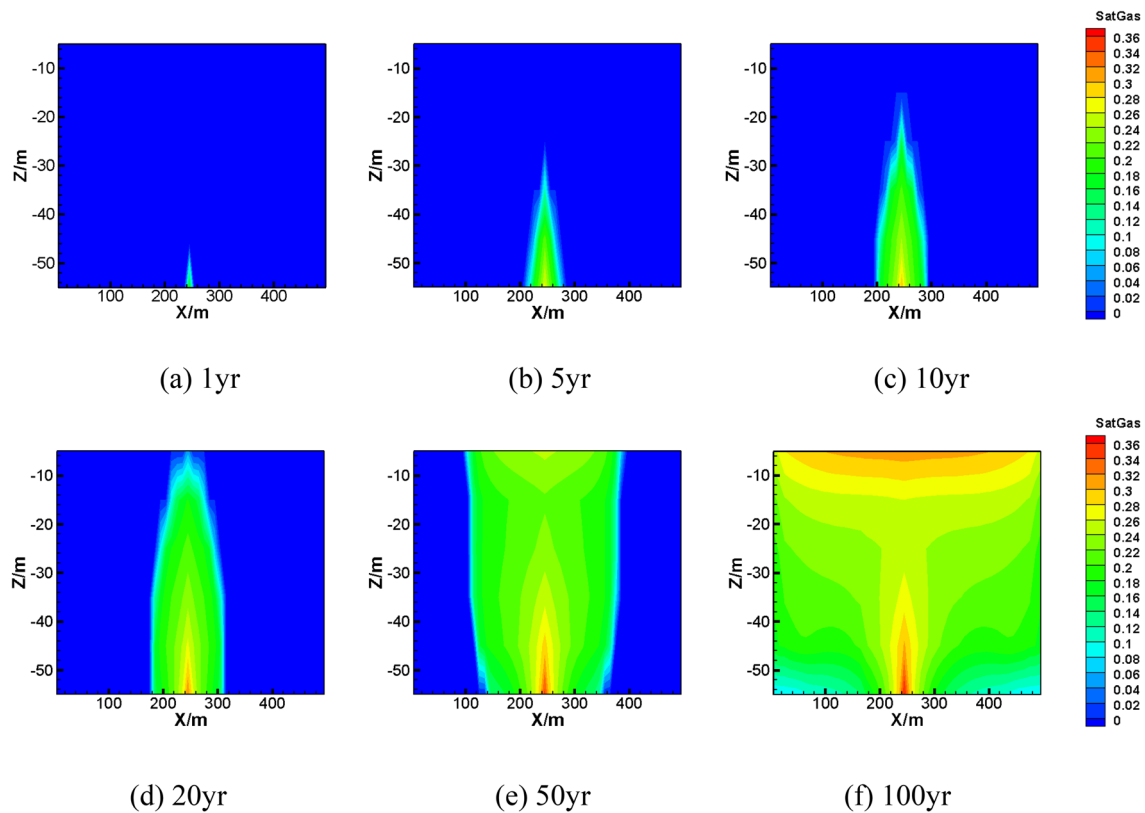| Component	Measured initial concentration (mol/L)	Equilibrium concentration (mol/L)
K^+	4.462×10^{-5}	4.3634×10^{-5}
Ca^{2+}	2.156×10^{-3}	3.2542×10^{-4}
Na^+	5.111×10^{-3}	5.0622×10^{-1}
Mg^{2+}	2.295×10^{-3}	3.7282×10^{-13}
Fe^{2+}	1.893×10^{-5}	2.4642×10^{-12}
HCO_3^-	4.025×10^{-4}	5.4955×10^{-1}
SO_4^{2-}	2.515×10^{-3}	2.3002×10^{-3}
AlO_2^-	5.085×10^{-7}	1.0286×10^{-10}
Cl^-	3.364×10^{-3}	3.0714×10^{-3}
pH	7.95	6.67

Fig. 3 Spatial distribution of CO_2 gas saturation

Results and discussion

Change of CO_2 concentration in groundwater

As shown in Fig. 3, after CO_2 migrates to groundwater, because the density of CO_2 is smaller than the density of water, CO_2 will migrate upward under buoyancy and gradually diffuse to the surroundings. As CO_2 gradually diffuses, the CO_2 gas saturation in the groundwater formation gradually increases. By 100 years, the CO_2 gas saturation at the leaking point is about 0.36(Fig. 5a). CO_2 basically diffuses into the entire area and gather at the top of groundwater (Fig. 3f). A fraction of CO_2 will dissolve in groundwater and participate in water–rock interactions. As CO_2 gradually migrates, the region with dissolved CO_2 in groundwater gradually expands (Fig. 4). The dissolved CO_2 concentration increases gradually at the point source of CO_2 injection. By 10 years the concentration of dissolved CO_2 changes little at the leaking point. By 100 years, the concentration of CO_2 dissolved at the point source of CO_2 is about 0.38 mol/L (Fig. 5b).

Chemical reaction in groundwater and change of mineral volume fraction

With the gradual migration of CO_2, the amount of CO_2 dissolved in groundwater continues to increase, and the spatial distribution of pH gradually expands (Fig. 6), resulting in a significant decrease in the pH value of groundwater and an increase in formation porosity (Fig. 7). By 100 years, the pH of groundwater has decreased from 6.67 to about 5.3 (Fig. 8a), and the chemical composition of groundwater is greatly affected. The porosity of the formation increases in 0–10 years, and when the mineral dissolution and precipitation reach a steady state, the porosity basically remains unchanged. By 100 years, formation porosity is approximately 0.20027 (Fig. 8b). The main reason for the decrease in pH value of groundwater is that CO_2 dissolves in groundwater to form carbonic acid, which is unstable and decomposes into H^+ and HCO_3^-. The reaction equations are as follows.
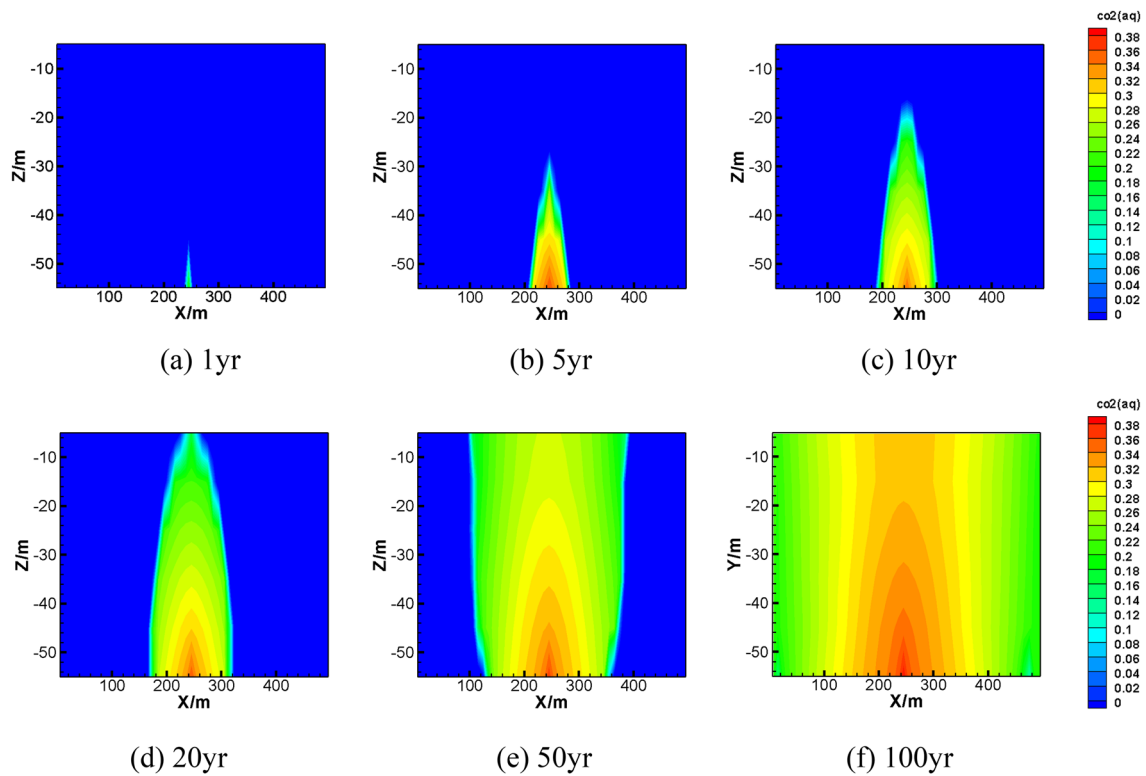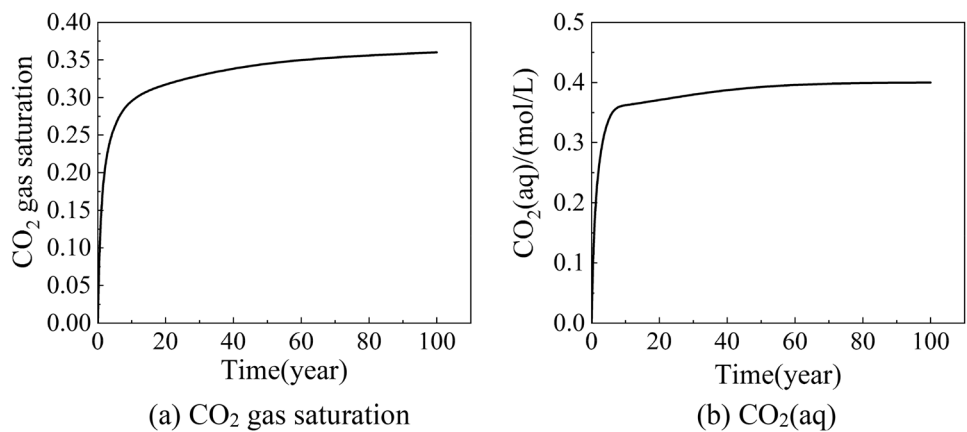
$$CO_2(gas) \rightleftharpoons CO_2(aq), \tag{6}$$

$$CO_2(aq) + H_2O \rightleftharpoons H_2CO_3, \tag{7}$$

$$H_2CO_3 \rightleftharpoons H^+ + HCO_3^-, \tag{8}$$

Fig. 4 Spatial distribution of dissolved CO_2

Fig. 5 Change in CO_2 concentration at the leaking point over time

(a) CO_2 gas saturation

(b) CO_2(aq)

$$HCO_3^- \rightleftharpoons H^+ + CO_3^{2-}. \tag{9}$$

The change in volume fraction (abundance) of mineral is defined by the following formula.

$$\frac{V_1 - V_0}{V_0}, \tag{10}$$

where V_0 is the initial volume fraction of mineral, V_1 is the volume fraction of mineral at a given time t. Negative values indicate dissolution, positive values indicate precipitation.

CO_2 migration to groundwater changes the acidity of the groundwater and the original water chemistry, leading to dissolution of calcite, oligoclase, K-feldspar, chlorite and hematite (Fig. 9a). The volume fraction of calcite remains almost unchanged after 10 years. The volume fractions of oligoclase, K-feldspar and chlorite gradually decrease, while
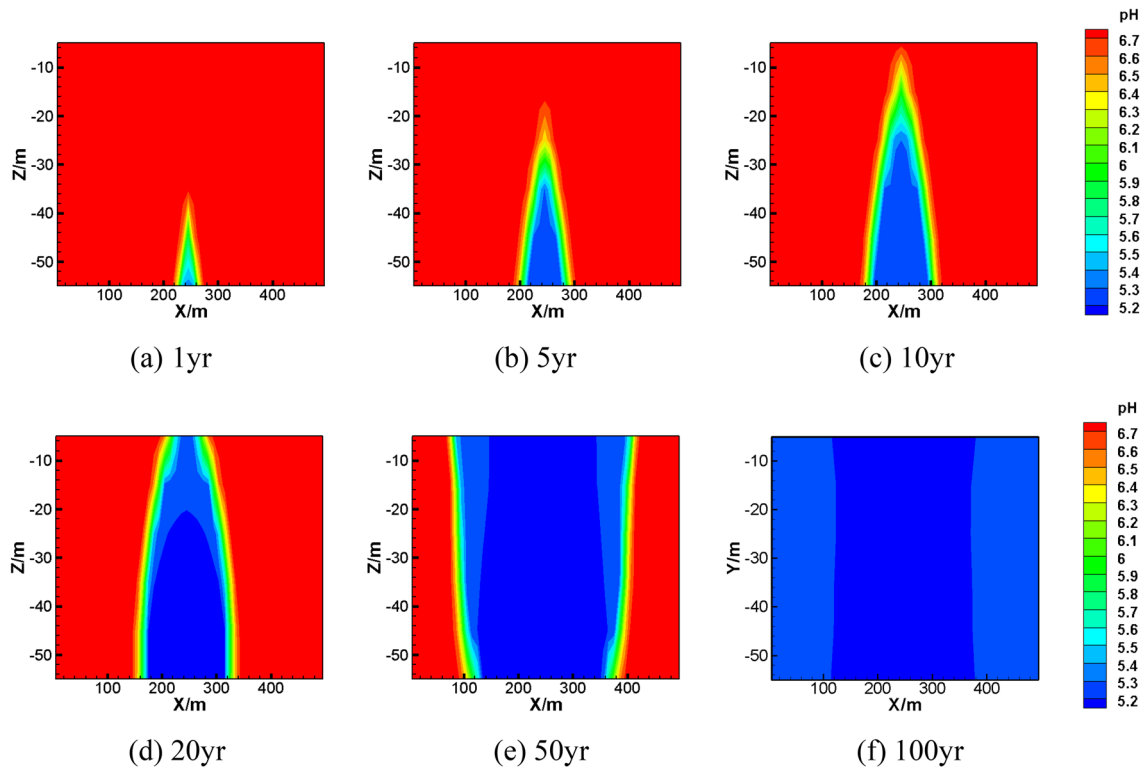
Fig. 6 Spatial distribution of pH
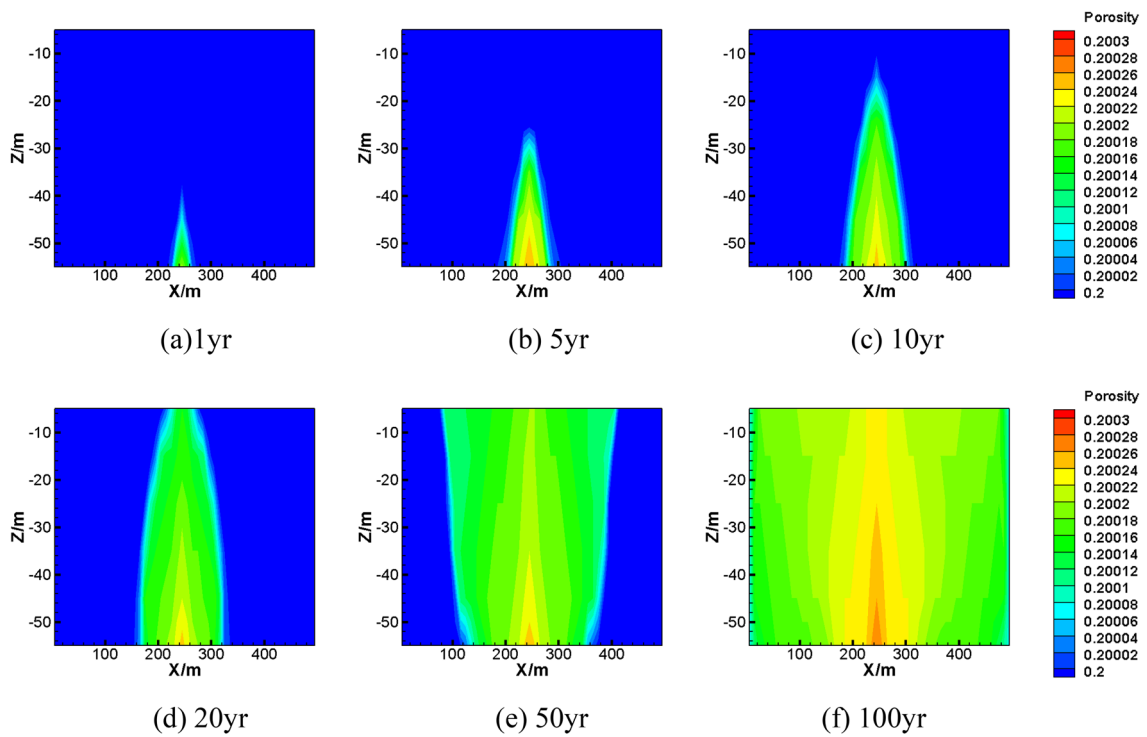
Fig. 7 Spatial distribution of porosity

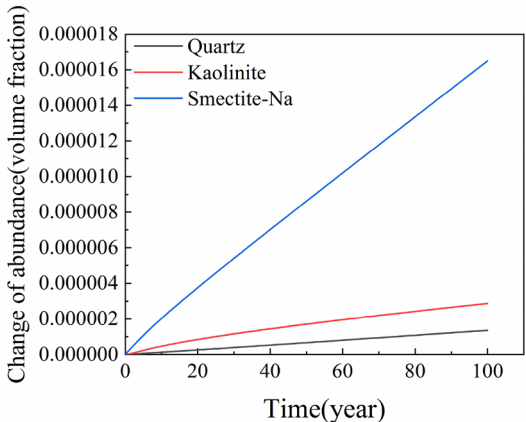**Fig. 8** Changes in pH and porosity at the leaking point over time

(a) pH

(b) Porosity

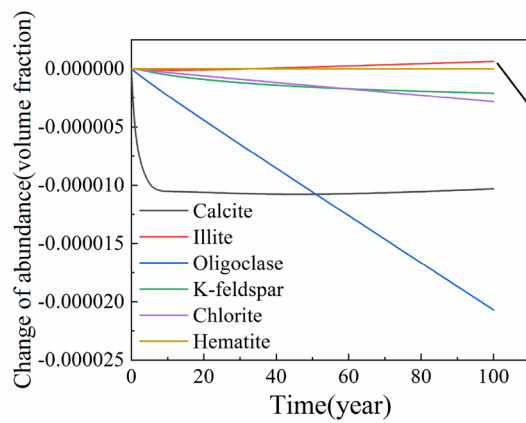(a) Dissolved primary minerals

(b) Illite

(c) Precipitated primary minerals

(d) Secondary minerals
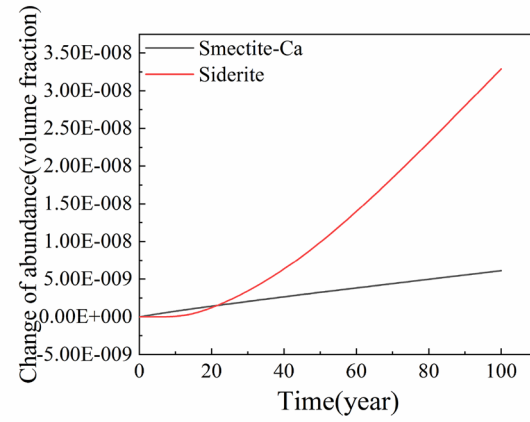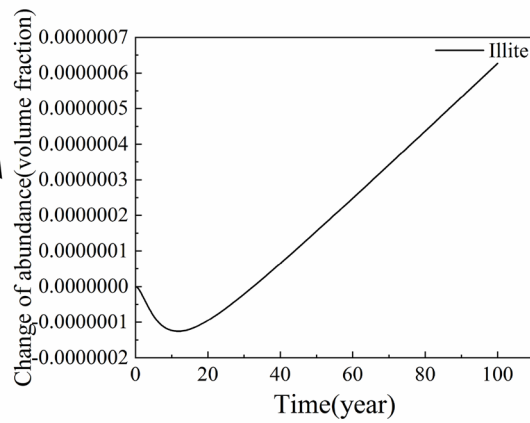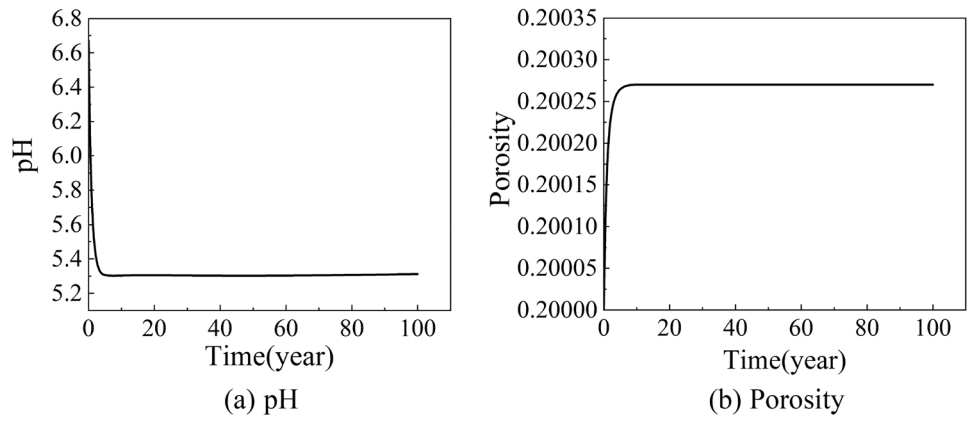
Fig. 9 Changes in mineral volume fraction (Note: negative value represents mineral dissolution, positive value represents mineral precipitation)

illite begins to precipitate after 10 years (Fig. 9b). The dissolution reactions are as follows:

$$CaCO_3(\text{Calcite}) + H^+ \rightarrow Ca^{2+} + HCO_3^-, \tag{11}$$
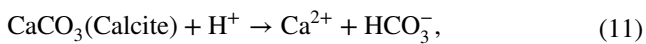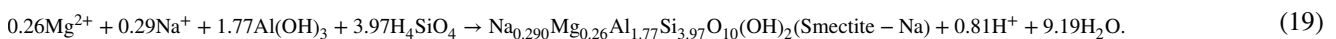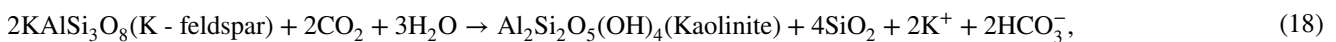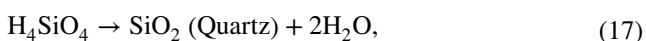
$$K_{0.6}Mg_{0.25}Al_{1.8}\left(Al_{0.5}Si_{3.5}O_{10}\right)(OH)_2(\text{Illite}) + 8H^+ + 5H_2O + 0.6K^+ + 0.25Mg^{2+} + 2.3Al^{3+} + 3.5SiO_2(\text{aq}), \tag{12}$$

$$CaNa_4Al_6Si_{14}O_{40}(\text{Oligoclase}) + 24H^+ \rightarrow Ca^{2+} + 4Na^+ + 6Al^{3+} + 14SiO_2(\text{aq}) + 12H_2O, \tag{13}$$

$$KAlSi_3O_8(\text{K - feldspar}) + 4H^+ \rightarrow K^+ + Al^{3+} + 3SiO_2(\text{aq}) + 2H_2O, \tag{14}$$

$$2Mg_{2.5}Fe_{2.5}Al_2Si_3O_{10}(OH)_8(\text{Chlorite}) + 20H^+ \rightarrow 5Mg^{2+} + 5Fe^{2+} + 4Al(OH)_3 + 6H_4SiO_4, \tag{15}$$

$$Fe_2O_3(\text{Hematite}) + 6H^+ \rightarrow 2Fe^{3+} + 3H_2O. \tag{16}$$
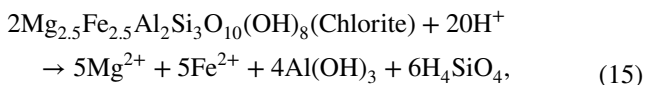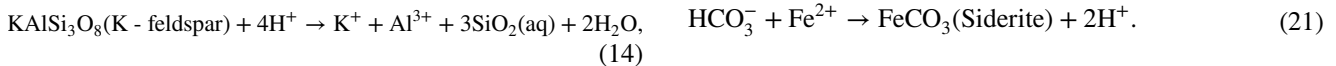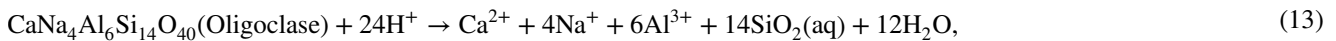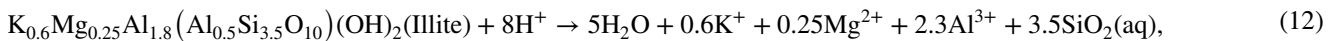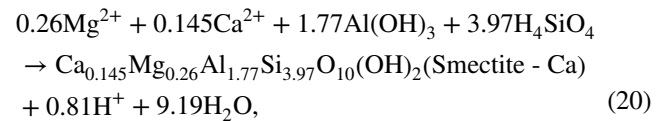
The dissolution of minerals consumes H^+ in the groundwater, alleviating the pH value of the groundwater, and leads to precipitation of secondary minerals. When the dissolved CO_2 in groundwater gradually increases, K-feldspar is gradually transformed into kaolinite. In addition, due to the massive dissolution of oligoclase and chlorite, the concentration of Na^+ and Mg^{2+} in the groundwater increases significantly, resulting in the precipitation of smectite-Na. Figure 9c shows that the mineral volume fraction of quartz, kaolinite and smectite-Na increases gradually, and the amount of mineral precipitation increases accordingly, among which the volume fraction of smectite-Na changes the most. By 100 years, the volume fraction of smectite-Na changes by about 1.65×10^{-5}, while the volume fraction of hematite remains almost unchanged. The precipitation reactions occur as follows.

$$H_4SiO_4 \rightarrow SiO_2 \text{ (Quartz)} + 2H_2O, \tag{17}$$

$$2KAlSi_3O_8(\text{K - feldspar}) + 2CO_2 + 3H_2O \rightarrow Al_2Si_2O_5(OH)_4(\text{Kaolinite}) + 4SiO_2 + 2K^+ + 2HCO_3^-, \tag{18}$$

$$0.26Mg^{2+} + 0.29Na^+ + 1.77Al(OH)_3 + 3.97H_4SiO_4 \rightarrow Na_{0.290}Mg_{0.26}Al_{1.77}Si_{3.97}O_{10}(OH)_2(\text{Smectite} - Na) + 0.81H^+ + 9.19H_2O. \tag{19}$$

The dissolution and precipitation of the initial minerals lead to significant changes in the concentration of chemical components in the groundwater, which then recombine to form secondary minerals. In 100 years, the secondary minerals are mainly smectite-Ca and siderite. As shown in Fig. 9d, the volume fraction of smectite-Ca and siderite gradually increases, and the volume fraction of siderite changes the most. By 100 years, the volume fraction of siderite changes about 3.29×10^{-8}. The reactions that occur are as follows:

$$0.26Mg^{2+} + 0.145Ca^{2+} + 1.77Al(OH)_3 + 3.97H_4SiO_4 \rightarrow Ca_{0.145}Mg_{0.26}Al_{1.77}Si_{3.97}O_{10}(OH)_2(\text{Smectite - Ca}) + 0.81H^+ + 9.19H_2O, \tag{20}$$

$$HCO_3^- + Fe^{2+} \rightarrow FeCO_3(\text{Siderite}) + 2H^+. \tag{21}$$

Changes in the concentration of chemical components in groundwater

Figure 10a shows that the concentration of K^+ gradually increases at the point source of CO_2 leaking. The increase in K^+ concentration is mainly due to the dissolution of K-feldspar and illite. Illite begins to precipitate after 10 years, which consumes K^+, making the concentration of K^+ increase slowly after 10 years. By 100 years, the concentration of K^+ at the leaking point is 1.67×10^{-4} mol/L. The dissolution of calcite and oligoclase for the generation of secondary mineral smectite-Ca offers a large amount of Ca^{2+}. In the initial time of CO_2 leakage, the concentration of Ca^{2+} increases significantly. By 10 years, the concentration of Ca^{2+} is 2.09×10^{-3} mol/L at the leaking point, after 10 years, the concentration of Ca^{2+} increases more slowly. By 100 years, the concentration of Ca^{2+} is 2.18×10^{-3} mol/L (Fig. 10b) at the leaking point. The change trend of the concentration of Ca^{2+} is basically the same as that of calcite. The dissolution of oligoclase significantly increases the concentration of Na^+ in groundwater, while the formation of smectite-Na consumes part of Na^+. Figure 9a, c shows that the volume fraction change of oligoclase is about 2.07×10^{-5}, and the volume fraction of smectite-Na is about 1.65×10^{-5} at 100 years. Since the initial volume fraction of oligoclase is much larger than that of smectite-Na, the concentration of Na^+ gradually increases (Fig. 10c).

Figure 10d shows that the concentration of Mg^{2+} increases first and then decreases. The dissolution of illite and chlorite significantly increase the concentration of Mg^{2+} in groundwater, and the precipitation of smectite-Na and smectite-Ca consume part of Mg^{2+}. It can be seen from Fig. 9c, d
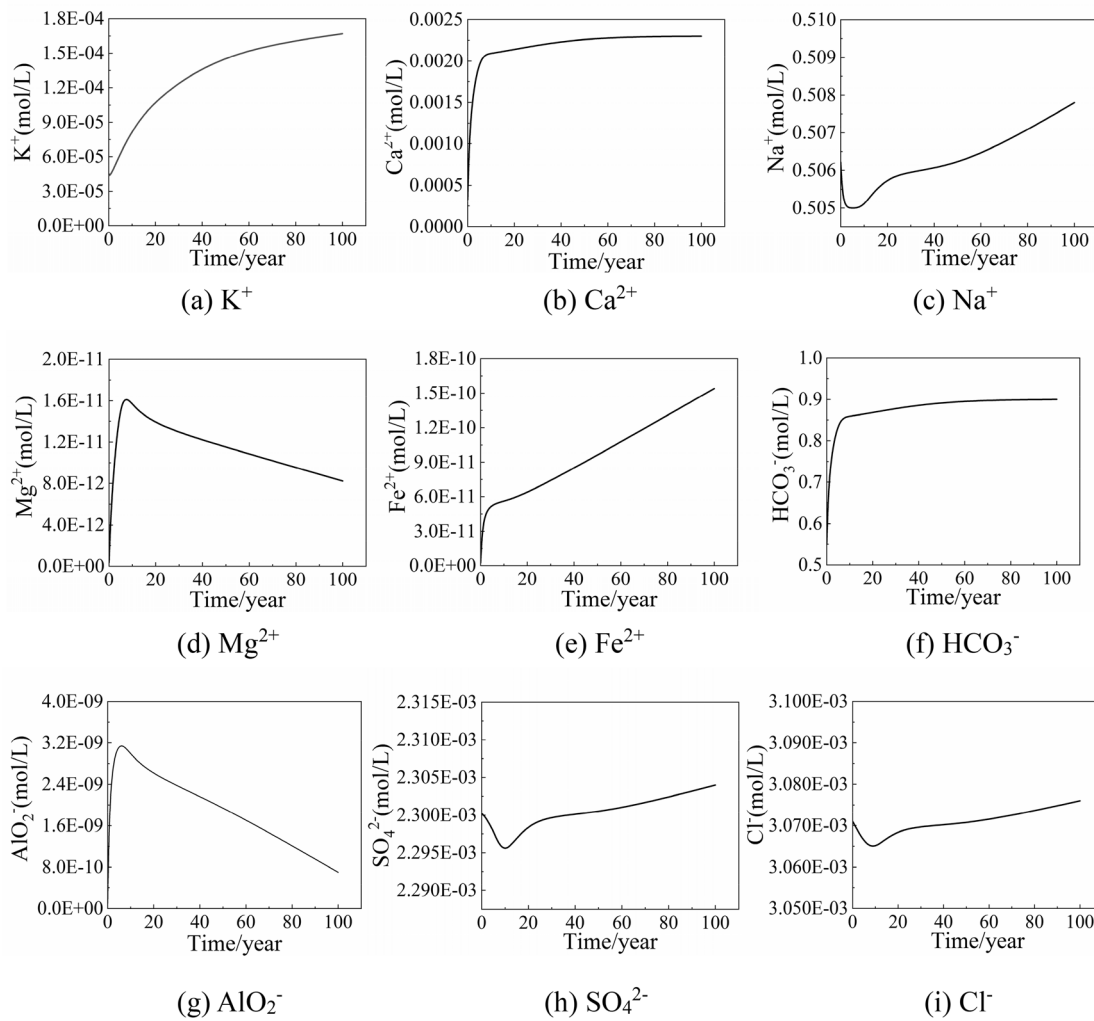
Fig. 10 Changes in chemical composition concentration with time at the leakage point

the volume fraction change of smectite-Na and smectite-Ca increase significantly and consume a large amount of Mg^{2+}. Therefore, the concentration of Mg^{2+} decreases significantly after 10 years, but it is still higher than the initial value, indicating that the content of Mg^{2+} produced by the dissolution of illite and chlorite is still greater than the Mg^{2+} consumed by smectite-Na and smectite-Ca precipitation. It can be seen from Fig. 10e the concentration of Fe^{2+} increases significantly. The dissolution of chlorite provides a large amount of Fe^{2+} for the precipitation of siderite. Comparing Fig. 9a, b, it can be seen that the change in the volume fraction of chlorite is 2–3 orders of magnitude higher than the change in the volume fraction of siderite. In 10 years, the volume fraction of siderite changes significantly. Therefore, the concentration of Fe^{2+} increases significantly in 0–10 years. Due to the increase in the amount of siderite precipitation and the consumption of part of Fe^{2+}, the increasing trend of Fe^{2+} began to slow down.

The change of HCO_3^- concentration is partly caused by the decomposition of carbonic acid, and partly by the dissolution of calcite and the precipitation of siderite. According to Fig. 10f, by 10 years, the concentration of HCO_3^- is 0.86 mol/L at the leaking point, and from the 10 years, the concentration of HCO_3^- changes little. Comparing Fig. 9a, d, it can be seen that the variation of the volume fraction of calcite is significantly greater than that of siderite, and the variation trend of the concentration of HCO_3^- is basically similar to that of the dissolved CO_2 and Ca^{2+} in groundwater. As can be seen from Fig. 10g, the concentration of AlO_2^- increases first and then decreases. The increase of AlO_2^- concentration is mainly due to the precipitation of illite. In addition, the dissolved CO_2 in the water also reacts with part of AlO_2^- (Formula (22)), leading to the decrease of AlO_2^- concentration, but the concentration of AlO_2^- is still higher than the initial value. Due to SO_4^{2-} and Cl^- in the groundwater is not involved in the mineral dissolution and precipitation reaction, therefore, the

Fig. 11 CO$_2$ geological storage safety monitoring indicators

(a) 10 years

(b) 100 years
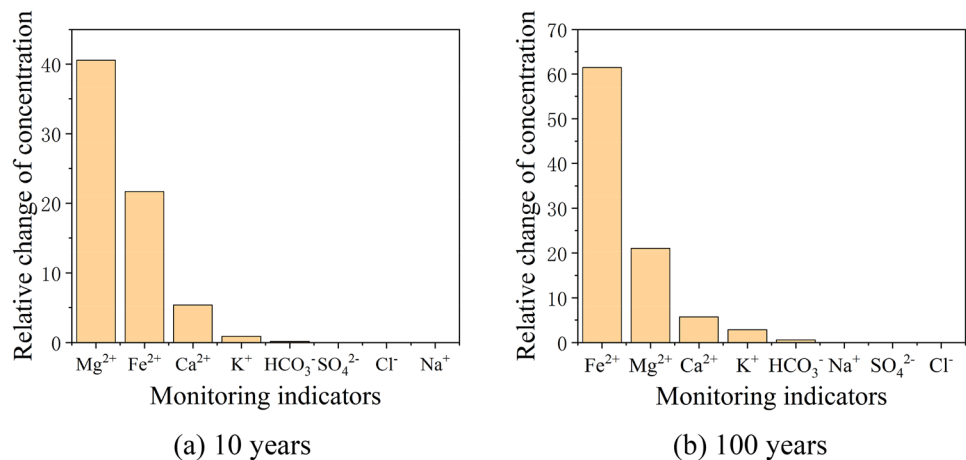
concentration of SO$_4^{2-}$ and Cl$^-$ change very little, and basically maintain at the initial value (Fig. 10h, i).

$$AlO_2^- + CO_2 + 2H_2O \rightarrow Al(OH)_3 + HCO_3^-. \tag{22}$$
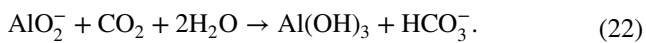
Monitoring indicators

As the pH of groundwater decreases significantly with CO$_2$ leakage, the acidity of groundwater increases significantly, and the monitoring of pH value is more convenient and intuitive, therefore, we should focus on monitoring the change characteristics of the pH value of groundwater. It is recommended to lay an in-situ online monitor in the target aquifer to monitor the change characteristics of the pH of groundwater. The frequency of in-situ online monitoring is recommended to be once every 10 min, and sampling monitoring is recommended to be once a month. By comprehensively improving the monitoring frequency of groundwater, the changes of groundwater monitoring indicators can be timely and accurately grasped. The data obtained from monitoring should be compared with the previous environmental background value to eliminate fluctuations in monitoring indicators caused by non-CO$_2$ leakage such as environmental factors and human activities, so as to avoid the wrong judgment of CO$_2$ leakage. If the pH of groundwater is abnormal, it is highly likely to be caused by CO$_2$ leakage, and remedial measures should be taken immediately.

Due to the small changes in formation porosity, it is not suitable as a monitoring indicators. As AlO$_2^-$ has a strong ability to bind H$^+$, it is very easy to form Al(OH)$_3$ precipitation, making it is not suitable as a monitoring indicator. The relative change of ion concentration in groundwater is calculated by the following formula.

$$R = \frac{|C_1 - C_0|}{C_0}, \tag{23}$$

where C_1 is the ion concentration at a given moment, (mol/L); C_0 is the initial ion concentration, (mol/L).

Figure 11 shows that the concentrations of Fe^{2+}, Mg^{2+} and Ca^{2+} in groundwater change significantly after 10 and 100 years of CO$_2$ leaking. The concentrations of K$^+$ and HCO$_3^-$ change slightly, while the concentrations of Na$^+$, Cl$^-$ and SO$_4^{2-}$ remain almost unchanged. Therefore, it is recommended to adopt Fe^{2+}, Mg^{2+} and Ca^{2+} as important monitoring indicators of CO$_2$ leakage. Ion concentration is mainly monitored by sampling. It is recommended to take samples once a month before CO$_2$ injection and storage, twice a month during CO$_2$ injection and storage, and once a month in the later stage of CO$_2$ injection and storage. In the monitoring process, the sampling frequency and analysis intensity should be adjusted according to the actual situation, and the CO$_2$ leakage situation should be judged jointly with the monitoring instrument.

These indicators are recommended to be monitored to detect CO$_2$ in time and provide early warnings. Once data abnormalities are found, corresponding measures should be taken. In addition, some monitoring indicators (such as conductivity, temperature and pressure, etc.) can be appropriately added based on the actual situation on site, and the monitoring indicator system can be further improved on the basis of accurate data.

Conclusions

In this work, the multi-phase reaction transport code TOUGHREACT-OMP/ECO2N is used to model the influence of CO$_2$ migration on shallow groundwater. The following conclusions are made from our simulations.

1. After CO$_2$ migrates to groundwater, it migrates upward due to buoyancy in gaseous form and gradually diffuses to the surroundings, and the CO$_2$ gas saturation

in groundwater gradually increases. A fraction of CO_2 will be dissolved in the groundwater. As the dissolved CO_2 gradually increases, the acidity of the groundwater is significantly increased and the pH is significantly reduced, causing dissolution/precipitation of the initial minerals, resulting in a slight increase in the porosity of the formation.

2. The dissolved minerals are calcite, illite, oligoclase, K-feldspar, chlorite and hematite; the precipitated minerals are quartz, kaolinite and smectite-Na. The secondary minerals are siderite and smectite-Ca.

3. The dissolution and precipitation of minerals change the concentration of chemical components in the groundwater. The concentrations of K^+ and Fe^{2+} in the groundwater gradually increase. The concentrations of Ca^{2+} and HCO_3^- remain basically unchanged after increasing to a certain value. The concentration of Mg^{2+} and AlO_2^- increase first and then decrease, but is still higher than the initial value. The concentration of Na^+, SO_4^{2-} and Cl^- do not change much.

4. It is suggested to choose pH as an important indicator to judge whether CO_2 leakage into groundwater during geological storage. At the same time, the changes of Fe^{2+}, Mg^{2+}, and Ca^{2+} should be monitored. These indicators could provide early warning of CO_2 leakage.

Declarations

Conflict of interest All authors certify that they have no affiliations with or involvement in any organization or entity with any financial interest or non-financial interest in the subject matter or materials discussed in this manuscript.

References

Aines RD, Leach MJ, Weisgraber TH, Simpson MD, Friedmann SJ, Bruton CJ (2009) Quantifying the potential exposure hazard due to energetic releases of CO_2 from a failed sequestration well. Energy Proc 1(1):2421–2429. https://doi.org/10.1016/j.egypro.2009.02.003

Apps JA, Zheng L, ZhangY XuTF, Birkholzer JT (2010) Evaluation of potential changes in groundwater quality in response to CO_2 leakage from deep geologic storage. Transport Porous Med 82(1):215–246. https://doi.org/10.1007/s11242-009-9509-8

Cao F, Eskin D, Leonenko Y (2021) Modeling of carbon dioxide dissolution in an injection well for geologic sequestration in aquifers. Energy 221(7):119780. https://doi.org/10.1016/j.energy.2021.119780

Carroll S, Hao Y, Aines R (2009) Geochemical detection of carbon dioxide in dilute aquifers. Geochem T 10(1):1–18. https://doi.org/10.1186/1467-4866-10-4

Chen K (2013) The impact of CO_2 leakage from reservoir on the water quality of the shallow aquifer. Dissertation, Jilin University, CN

Corey AT (1954) The interrelation between gas and oil relative permeabilities. Prod Mon 01:38–41

Du SH, Su XS, Zheng LG (2012) Advances in deep CO_2 leakage impact on shallow groundwater quality. Adv Water Sci 023(006):875–880. https://doi.org/10.14042/j.cnki.32.1309.2012.06.013

Fahrner S, Schaefer D, Dahmke A (2011) Reactive transport modeling to assess geochemical monitoring for detection of CO_2 intrusion into shallow aquifers. Energy Proc 4:3155–3162. https://doi.org/10.1016/j.egypro.2011.02.230

Gardiner JB, Capo RC, Newell DL, Stewart BW, Hakala JA (2021) Tracking natural CO_2 migration through a sandstone aquifer using Sr, U and C isotopes: Chimayó, New Mexico, USA. Int J Greenh Gas Con 104:103209. https://doi.org/10.1016/j.ijggc.2020.103209

Keating EH, Fessenden J, Kanjorski N, Koning DJ, Pawar R (2010) The impact of CO_2 on shallow groundwater chemistry: observations at a natural analog site and implications for carbon sequestration. Environ Earth Sci 60(3):521–536. https://doi.org/10.1007/s12665-009-0192-4

Keating EH, Hakala JA, Viswanathan H, Carey JW, Pawar R, Guthrie GD, Fessenden-Rahn J (2013) CO_2 leakage impacts on shallow groundwater: Field-scale reactive-transport simulations informed by observations at a natural analog site. Appl Geochem 30(Complete):136–147. https://doi.org/10.1016/j.apgeochem.2012.08.007

Kharaka YK, Thordsen JJ, Kakouros E, Ambats G, Herkelrath WN, Beers SR, Birkholzer JT, Apps JA, Spycher NF, Zheng L (2010) Changes in the chemistry of shallow groundwater related to the 2008 injection of CO_2 at the ZERT field site, Bozeman. Montana Environ Earth Sci 60(2):273–284. https://doi.org/10.1007/s12665-009-0401-1

Kim J, Lee S, Ha S, Joun W, Ju YJ, Lee K (2020) Natural ^{222}Rn as a tracer of mixing and volatilization in a shallow aquifer during a CO_2 injection experiment. Hydrol Process 34(26):5417–5428. https://doi.org/10.1002/hyp.13953

Lasaga AC (1984) Chemical kinetics of water-rock interactions. J Geophys Res 89:4009–4025. https://doi.org/10.1029/JB089iB06p04009

Lasaga AC, Soler JM, Ganor J, Burch TE, Nagy KL (1994) Chemical weathering rate laws and global geochemical cycles. Geochim Cosmochim Acta 58:2361–2368. https://doi.org/10.1016/0016-7037(94)90016-7

Little MG, Jackson RB (2010) Potential impacts of leakage from deep CO_2 geo-sequestration on overling freshwater aquifers. Environ Sci Technolog 44:9225–9232. https://doi.org/10.1021/es102235w

Little MG, Jackson RB (2011) Response to comment on "Potential impacts of leakage from deep CO_2 geo-sequestration on overlying freshwater aquifers." Environ Technol 45(7):3175–3176. https://doi.org/10.1021/es200421f

Lu J, Partin JW, Hovorka SD, Wong C (2010) Potential risks to freshwater resources as a result of leakage from CO_2 geological storage: a batch-reaction experiment. Environ Earth Sci 60(2):335–348. https://doi.org/10.1007/s12665-009-0382-0

Meer L (1992) Investigations regarding the storage of carbon dioxide in aquifers in the Netherlands. Energ Convers Manage 33(5–8):611–618. https://doi.org/10.1016/0196-8904(92)90063-3

Newell DL, Larson TE, Perkins G, Pugh JD, Stewart BW, Capo RC, Trautz RC (2014) Tracing CO_2 leakage into groundwater using carbon and strontium isotopes during a controlled CO_2 release field test. Int J Greenh Gas Con 29:200–208. https://doi.org/10.1016/j.ijggc.2014.08.015

Oldenburg CM, Jordan PD, Nicot JP, Nicot JP, Mazzoldi A, Gupta AK, Bryant SL (2011) Leakage risk assessment of the In Salah CO_2 storage project: applying the certification framework in a

dynamic context. Energy Proc 4:4154–4161. https://doi.org/10.1016/j.egypro.2011.02.360

Palandri J, Kharaka YK (2004) A compilation of rate parameters of water-mineral interaction kinetics for application to geochemical modeling. US Geology Surv Open File Report 2004-1068

Pruess K, Oldenburg C, Moridis G (1999) TOUGH2 User's Guide, Version 2.0. LBL-43134, Lawrence Berkeley National Laboratory, Berkeley, CA. https://doi.org/10.2172/751729

Pruess K, Garcia J, Kovscek T, Oldenburg C, Rutqvist J, Steefel C, Xu T (2004) Code intercomparison builds confidence in numerical simulation models for geologic disposal of CO_2. Energy 29(9/10):1431–1444. https://doi.org/10.1016/j.energy.2004.03.077

Quattrocchi F, Barbieri M, Bencini R, Cinti D, Durocher K, Galli G (2005) Strontium isotope (^{87}Sr/^{86}Sr) chemistry in produced oil-field waters: the iea weyburn CO_2 monitoring and storage project. Greenh Gas Control Technol 65:2111–2114. https://doi.org/10.1007/1-4020-4471-2_20

Steefel CI, Lasaga AC (1994) A coupled model for transport of multiple chemical species and kinetic precipitation/dissolution reactions with applications to reactive flow in single phase hydrothermal system. Am J Sci 294:529–592. https://doi.org/10.2475/ajs.294.5.529

Van Genuchten MT (1980) A closed-form equation for predicting the hydraulic conductivity of unsaturated soils. Soil Sci Soc Am J 44(5):892–898. https://doi.org/10.2136/sssaj1980.03615995004400050002x

Wang S, Jaffe PR (2004) Dissolution of a mineral phase in potable aquifers due to CO_2 releases from deep formations; effect of dissolution kinetics. Energ Convers Manage 45(18–19):2833–2848. https://doi.org/10.1016/j.enconman.2004.01.002

Xie J, Wei N, Wu LZ, Zhang KN, Xu M (2017) Progress in leakage study of geological CO_2 storage. Rock Soil Mech S1:187–194. https://doi.org/10.16285/j.rsm.2017.S1.021

Xu TF (2001) Modeling multiphase non-isothermal fluid flow and reactive geochemical transport in variably saturated fractured rocks: 1. Methodology. AM J Sci 301(1):16–33. https://doi.org/10.2475/ajs.301.1.16

Xu TF, Sonnenthal E, Spycher N, Pruess K (2006) TOUGHREACT-A simulation program for non-isothermal multiphase reactive geochemical transport in variably saturated geologic media: applications to geothermal injectivity and CO_2 geological sequestration. Comput Geosci-UK 32(2):145–165. https://doi.org/10.1016/j.cageo.2005.06.014

Xu TF, Kharaka YK, Doughty C, Freifeld BM, Daley TM (2010) Reactive transport modeling to study changes in water chemistry induced by CO_2 injection at the Frio-I Brine Pilot. Chem Geol 271(3–4):0–164. https://doi.org/10.1016/j.chemgeo.2010.01.006

Xu TF, Sonnenthal E, Spycher N, Zheng LG (2014) TOUGHREACT V3.0-OMP sample problems. Earth Sciences Division, Lawrence Berkeley National Laboratory University of California, Berkeley, CA, 94720

Zhang L, Parthasarathy H, Karamalidis A (2016) Investigation on arsenopyrite dissolution and As(III) migration under geologic carbon storage conditions: a numerical simulation approach. Greenh Gases. https://doi.org/10.1002/ghg.1651